Antarctic Science 8 (2): 209–217 (1996)

Atmospheric surface pressure over the interior of Antarctica

UWE RADOK[1], IAN ALLISON[2] and GERD WENDLER[3]

[1]CIRES, Campus Box 449, University of Colorado, Boulder, CO 80309, USA
[2]Antarctic CRC and Australian Antarctic Division, GPO Box 252C, Hobart 7001, Australia
[3]Geophysical Institute, University of Alaska, Fairbanks, AK 99775-0800, USA

Abstract: Atmospheric surface pressures on the East Antarctic ice sheet are examined as a contribution to a new regional climatology based on automatic weather stations (AWS). Monthly mean pressures along two meridional AWS lines show near the coast a semi-annual oscillation with equinoctial minima, which become submerged inland under a larger annual oscillation, asymmetrically shaped around a summer solstice peak. Such a peak could arise when air surrounding the ice sheet is heated and enabled to spread out over the ice. This concept has provided a classical prediction of the ice sheet's mean elevation; in this paper the theory is expressed in a more modern form. After the summer "flood" the vertical tropospheric circulation driving the progressive katabatic surface layer drainage from the ice sheet should create relatively higher pressures below the convergence region over the ice sheet center and lower pressures near the coast. In fact the observed mean monthly surface pressures decrease with elevation more slowly than follows from substituting the observed mean temperature-elevation gradients ("topographical lapse rates") in the hydrostatic equation. However, below the surface inversion along the sloping ice sheet surface the hydrostatic balance is shown to be governed by temperatures higher than observed at the surface. Hydrostatic pressures are calculated with climatic estimates of the inversion strength. Their differences from the observed monthly mean surface pressures represent non-hydrostatic residuals which can be added to pressures at the coast to form elevation-free ("sea level") pressure profiles. These show both the expected coastal troughs and high pressure over an ice sheet summit (Dome C).

Received 14 December 1995, accepted 3 January 1996

Key words: automatic weather stations, climatology, East Antarctica, ice sheet

Introduction

The establishment on the East Antarctic ice sheet of an automatic weather station (AWS) network (Allison & Morrissy 1983, Wendler *et al.* 1986) has made possible a regional surface climatology of the Antarctic interior (Allison *et al.* 1993). In this paper we use data from two lines of AWS, the IAGO (Interaction atmosphère-glace-océan) line (extending from Dumont d'Urville to Dome C) and the ANARE (Australian National Antarctic Research Expeditions) line (extending from Casey toward Vostok), to examine the pressures and to investigate relationships between elevation, temperature, and surface pressure along the ice sheet surface.

The locations of the AWS are given in Fig. 1 and Table I. Elevations in Table I generally represent satellite geodetic data (Transit or Global Positioning System (GPS)), corrected to orthometric heights with a broad-scale field of geoid-ellipsoid separation. The first AWS started operating in 1980, and observations up to and including those for 1990 have been available for this work. However, in some of the discussions below, the relatively complete AWS observations for the single year 1987 (omitting dubious data from GC46) will be used in order to reduce differences that could be introduced by station records of different lengths.

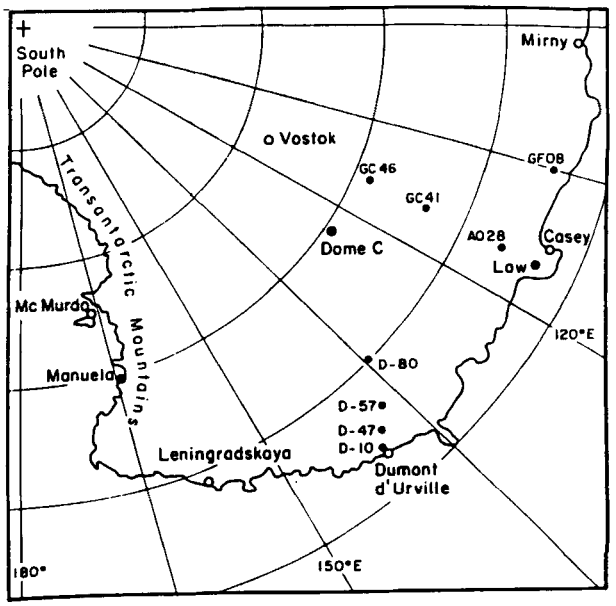

Fig. 1. The automatic weather stations (AWS) of the IAGO line, extending from Dumont d'Urville to Dome C, and of the ANARE line, extending from Casey to GC 46.

https://doi.org/10.1017/S0954102096000284 Published online by Cambridge University Press

Table I. Details of automatic and manned weather stations that provided the data used in this paper.

	Lat. S	Long. E	Elevation (m)	Distance from coast (km)
1) IAGO AWS line				
Dome C	74.50	123.00	3280	860
D80	70.02	134.72	2500	400
D57	68.18	137.52	2105	190
D47	67.38	138.72	1560	90
D10	66.70	139.80	240	10
2) ANARE AWS line				
GC46	74.13	109.83	3093	810
GC41	71.60	111.25	2759	530
A028	68.40	112.21	1625	230
Law	66.73	112.94	1366	80
3) Manned stations				
Vostok	78.45	106.87	3420	1365
Casey	66.27	110.63	15	1
Dumont d'Urville	66.67	140.02	43	-1

The annual evolution of surface pressure on the ice sheet

Table IIa lists monthly mean surface pressures for each AWS site. These means have been derived from all available measurements to the end of 1990. Table IIb lists the accompanying mean temperatures and Table IIc the data periods used for calculating the means (from Allison *et al.* 1993).

Figure 2 shows deviations from the annual mean pressures for the coastal stations of the two AWS lines and for the stations at the inland ends of the lines. At the low-level coastal station, D 10, a marked semi-annual component is in evidence. This component dominates Southern Hemisphere middle-latitude pressures; it was first reported by Schwerdtfeger & Prohaska (1956) and has since then been widely described and discussed (see e.g. van Loon 1967, Meehl 1991 and Tzeng *et al.* 1993). But, as previously shown by Wendler & Pook (1992), the semi-annual component is much less distinct in the pressures observed inland on Dome C. Figure 2 shows that it also disappears near the coast on Law Dome, the elevated AWS forming the beginning of the

Table II. Monthly mean data for AWS sites.

Station Month	D10	Law	D47	AO28	D57	D80	GC41	Dome C
a) Surface pressures (hPa)								
January	958.4	829.1	816.5	805.6	760.5	720.9	697.4	654.6
February	954.5	820.4	811.9	796.3	755.5	716.9	691.5	649.3
March	951.6	818.7	807.2	795.7	749.8	711.0	688.1	644.6
April	952.7	817.4	806.7	796.7	749.2	710.5	688.4	642.4
May	954.0	815.5	805.0	793.6	748.5	709.8	687.7	642.6
June	955.1	815.7	804.1	796.9	751.8	711.6	688.4	642.5
July	953.3	812.5	805.7	791.3	748.1	705.8	682.1	641.0
August	951.4	810.9	804.5	790.3	738.8	706.1	681.9	640.4
September	947.9	810.7	803.5	793.5	741.6	708.1	680.9	638.9
October	948.6	814.6	802.7	793.0	750.0	710.2	684.6	639.3
November	949.4	817.1	806.7	794.0	751.0	709.3	686.3	643.7
December	955.0	824.8	814.4	801.7	754.4	718.5	695.7	652.6
Year	952.7	817.3	807.4	795.7	749.9	711.6	687.7	644.3
b) Surface temperatures (°C) (from Allison *et al.* 1993)								
January	-2.9	-10.9	-14.1	-15.2	-17.2	-24.5	-25.7	-29.9
February	-6.3	-13.9	-17.6	-20.5	-21.7	-31.5	-34.4	-40.8
March	-11.6	-20.0	-23.8	-27.9	-29.4	-41.6	-45.3	-52.5
April	-15.5	-22.6	-28.2	-31.2	-34.4	-47.0	-50.9	-59.6
May	-17.2	-25.2	-30.9	-34.2	-39.2	-50.0	-55.0	-61.9
June	-18.0	-26.8	-31.7	-32.4	-33.4	-48.0	-53.5	-61.0
July	-18.7	-25.8	-31.1	-32.5	-36.7	-50.6	-51.6	-61.3
August	-19.0	-26.8	-30.4	-35.9	-41.8	-50.8	-52.7	-63.0
September	-16.6	-24.7	-27.4	-29.5	-34.3	-44.8	-49.2	-57.8
October	-15.1	-21.5	-25.6	-25.5	-32.0	-39.6	-44.1	-50.5
November	-9.2	-19.1	-20.9	-22.2	-24.3	-34.7	-35.7	-39.6
December	-3.7	-12.6	-14.5	-14.6	-18.9	-24.5	-25.2	-29.0
Year	-12.8	-20.8	-24.7	-26.8	-30.3	-40.6	-43.6	-50.6
c) Periods with good pressure and temperature data; incomplete years in parentheses (from Allison *et al.* 1993)								
	80 (81–84) 87–89	(86) 87–90	(84–86) 87 (88) 89	(86) 87–89 (90)	(81–87) 88	(83–85) 86–89	(84) 85–90	(80–81) 82 (84) 85–89

https://doi.org/10.1017/S0954102096000284 Published online by Cambridge University Press

ANARE line, whereas a stronger semi-annual component persists far inland at AWS GC41.

A harmonic analysis of surface pressures, observed during and after the IGY at high-level stations on the ice sheet (Schwerdtfeger 1984), yielded amplitudes for the semi-annual oscillation that are larger than those at the coast; but on the ice sheet the oscillation is overlain by a much larger annual oscillation of asymmetric shape around the pressure peak near the summer solstice. At Vostok the annual and semi-annual amplitudes are 6 and 4.2 hPa, respectively and together account for 99% of the total variance (Schwerdtfeger 1984); by contrast, the corresponding amplitudes at D10 are similar to the zonal mean amplitudes for 65°S, reported by van Loon (1967) as 0.6 and 2.8 hPa, respectively.

Now the physical factors responsible for the semi-annual pressure oscillation–radiation and temperature gradients, changes in the ocean surface energy budgets, and eddy transports, around 60°S (cf. e.g. Mehl 1991) – clearly lack relevance for conditions over the interior of Antarctica. There the semi-annual oscillation survives as a mathematical feature deforming an annual harmonic to the observed asymmetric shape of the annual pressure variation.

A physical mechanism that could lead directly to such an asymmetric pressure variation on the ice sheet was deduced by Meinardus (1909) from small differences between the January and July mean pressures averaged over the global surface, not including the ice sheet area. To preserve the total atmospheric mass, Meinardus had to postulate that the mean surface pressure p_1 over the ice sheet is 23 hPa higher in January than in July, while the mean pressure, p_0, at sea level along the Antarctic coast remains approximately the same in the two months (due to the semi-annual variation). Such an inland pressure rise could be created by the warming of the atmosphere which permits some of the tropospheric air previously blocked by the ice sheet to spread out across it.

With this interpretation Meinardus was able to obtain a first realistic estimate, "in excess of 2000 m", for the then unknown mean ice sheet elevation. His mathematical reasoning can be summarized in the following (modernized) form, using the hydrostatic equation

$$dp = -g\rho dz = -\frac{g}{R}\frac{p}{T}dz, \qquad (1)$$

where ρ is the air density, $T(°K)$ the temperature, and z the elevation above sea level; g is the acceleration of gravity, R the specific gas constant, and $-g/R$ = -0.0341°C m^{-1} the vertical temperature gradient ("lapse rate") in a constant-density atmosphere.

Integration of (1) over the layer between $z=0, p=p_0$ and the unknown mean elevation $z=h, p=p_1$ with mean temperatures T_{wi} for July and T_{su} for January, leads to

$$\ln p_0 - \ln p_1 = (g/R)(h/T_{wi}) \qquad (2a)$$

and

$$\ln p_0 - \ln(p_1 + \Delta p) = (g/R)(h/T_{su}), \qquad (2b)$$

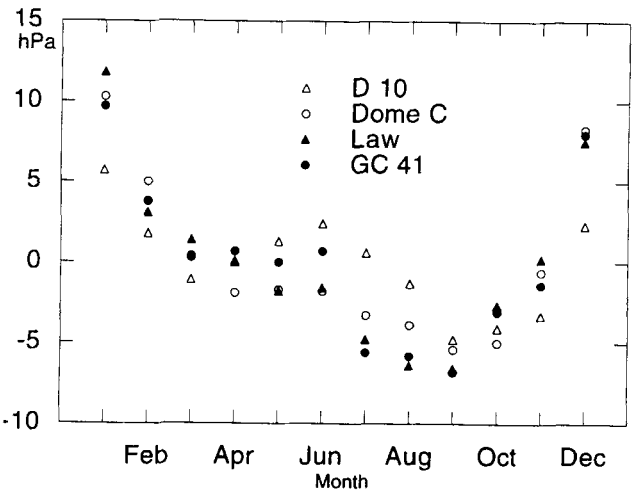

Fig. 2. Deviations of selected monthly mean surface pressures from their annual means. Open symbols: two IAGO stations; filled symbols: two ANARE stations. Circles are coastal stations, triangles inland stations.

where Δp is the pressure difference inferred above (23 mb). Subtracting equation (2a) from equation (2b) yields the following equation for h:

$$h = \left[(R/g)(T_{su}T_{wi})/(T_{su} - T_{wi})\right]\ln(1 + \Delta p/p_1) \qquad (3)$$

A matching value pair of the two unknown quantities h and p_1 can be found by entering (3) with an estimate for p_1 and using the resulting value of h and equation (2a) for a new p_1 estimate. Cycling between (3) and (2a), with Δp = 23 hPa and with the layer mean temperatures (T_{wi} = 235°K, T_{su} = 258°K) and sea level pressure (p_0 = 745 mmHg = 993.3 hPa) assumed by Meinardus, leads to h = 2464 m and p_1 = 695 hPa. The actual mean elevation of the grounded Antarctic ice sheet is close to 2100 m (Radok *et al.* 1986).

The "flooding" of the ice sheet in late spring would in general be effected by disturbances, but quasi-steady parallel rises of surface pressure and temperature have been recorded in some years by different AWS. An example occurred during November 1989 and is shown in Fig. 3. In these cases one might expect the pressure changes at higher AWS to trail those at lower AWS. The correlation coefficient between the pressures observed at D47 and D80 during November 1989 in fact reaches its maximum when the D80 pressures are compared with those preceding them at D47 by three hours. However, considering the horizontal and vertical distances involved (300 km and 1000 m), this time lag probably reflects a modified large-scale diurnal variation rather than the process envisioned by Meinardus. Records from other AWS and years may help to explain such spring events.

During the remainder of the year, synoptic systems and katabatic surface layer drainage gradually remove the summer's excess air from the ice sheet. The vertical tropospheric circulation driving the katabatic flow should

https://doi.org/10.1017/S0954102096000284 Published online by Cambridge University Press

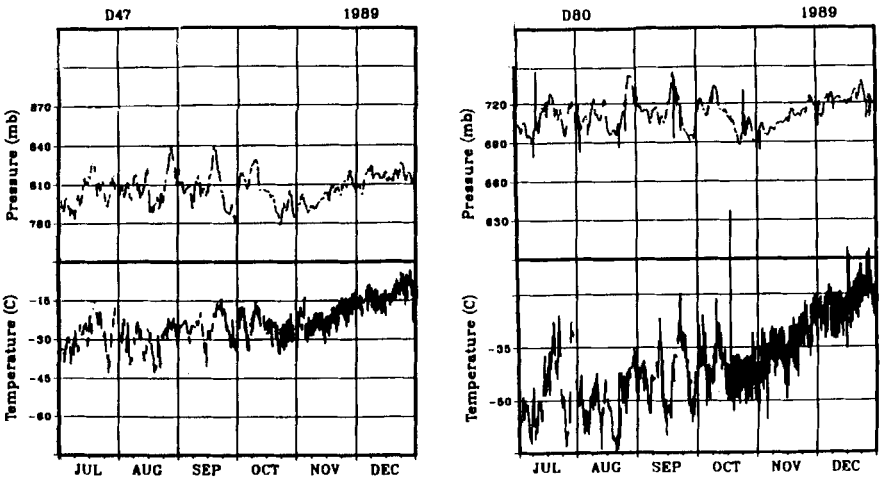

Fig. 3. Steady parallel rises in surface temperature and pressure that could reflect a "flooding" of the ice sheet at the end of Spring.

create relatively high pressures below the central region of mass convergence and relatively lower pressures near the coast. However, to verify these pressure anomalies the observed mean surface pressures must be freed from their strong dependence on elevation. This is attempted in the remainder of the paper.

Surface pressure and surface elevation

The dependence of surface pressure on station elevation is routinely removed by reducing surface pressures to mean sea level, assuming the surface temperature to persist down to that level. This gives acceptable results for elevations not exceeding some hundreds of meters; however, the adjusted pressures tend to grow to unrealistic values for higher elevations (cf. e.g. Schwerdtfeger 1984).

Along the ice sheet surface a temperature gradient ("topographical lapse rate") of -0.95°C/100 m has been recorded over the entire AWS levation range in summer; in winter gradients of -0.99°C/100 m prevail below 2000 m, and

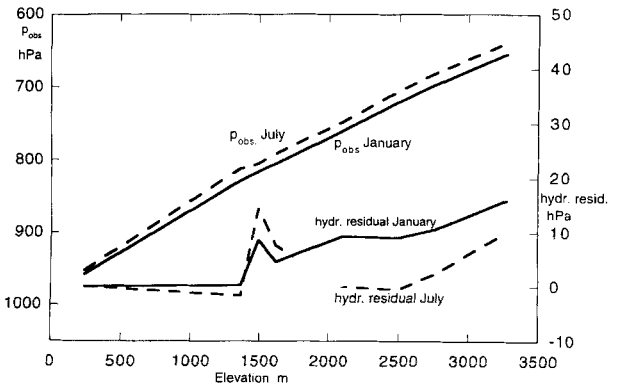

Fig. 4. Observed mean surface pressures p_{obs} for January and July along the combined line of AWS, and non-hydrostatic residuals p_{obs} - p_0. The p have been calculated with Equation (4b) and the observed topographic lapse rates for summer and winter (from Allison *et al.* 1993).

-1.87°C/100 m above 2000 m (Allison *et al.* 1993). These lapse rates can be used to obtain hydrostatic surface pressure estimates for the AWS elevations by integrating the constant-lapse rate form of the hydrostatic equation

$$dp = -\frac{g}{R}\frac{p}{(T_0 - \Gamma E)}dE \tag{4a}$$

where $\Gamma = dT/dE$ is the lapse rate, from near sea level (as well as from the AWS closest to the 2000 m level in winter). Figure 4 shows the differences between these hydrostatic pressure estimates,

$$p_0 = p_{sl}\left[1 - \frac{\Gamma E}{T_0}\right]^{\frac{g}{R\Gamma}} \tag{4b}$$

and the observed mean pressures along the combined line of AWS. With increasing elevation the hydrostatic estimates drop below the observed mean pressures. Similar results were previously obtained for both Antarctica and Greenland by Radok (1981).

Figure 4 suggests that realistic hydrostatic calculations should use higher-than-observed surface temperatures. This is supported by a re-examination of the hydrostatic balance along the ice sheet surface by Jenssen & Radok (1982). The details of this analysis (originally aimed at reconciling ice core temperature and elevation estimates) are given for the first time in Appendix A and take account of the temperature inversion usually encountered over the ice sheet surface, cf. Fig. 5. By allowing for different lapse rates along the vertical and along the sloping surface, the hydrostatic balance along the slope is shown to obey the hydrostatic equation (1) with a constant temperature $T^* = T_0T_z/T_1$:

$$dp_0 = -\frac{g}{R}\frac{p_0}{T_0}\frac{T_1}{T_z}dE = -\frac{g}{R}\frac{p_0}{T^*}dE \tag{5}$$

The factor T_z/T_1 is a measure of the horizontal temperature

https://doi.org/10.1017/S0954102096000284 Published online by Cambridge University Press

gradient through the surface inversion above the level of p_0 in Fig. 5. Dalrymple *et al.* (1966) have pointed out that the usually positive difference $T_z - T_1$ can maintain the persistent katabatic surface flow as a "thermal wind", even when calm conditions and a zero pressure gradient prevail above the inversion.

Assuming constant lapse rates between neighbouring AWS, integration of (5) over ΔE leads to

$$p_1 = p_0 \exp\left[-\frac{g\,\Delta E}{R\,T^*}\right] \qquad (6)$$

The key parameter is the free-air temperature T_z which is not available for the AWS sites and needs to be derived from upper air soundings and physical considerations, described in the next section.

Free-air temperatures over the ice sheet

One approximation to the free-air temperature T_z is provided by the temperature T_M at the top of the surface inversion usually encountered over the ice sheet. That temperature would be too high when the level of the next higher AWS (with surface pressure p_1) falls within the inversion above the lower station (with surface pressure p_0). The same applies when the elevation difference between the two stations exceeds the inversion thickness at the lower station. With T_M in place of T_z in calculating T^*, therefore, equation (6) minimizes the hydrostatic pressure decrease with elevation between the two stations considered.

A physical limit for the maximum rate of decrease is created by the vertical lapse rate γ which for a stable stratification must remain above –1°C/100 m. This limit is obtained with $T_{zmin} = T_0 - 0.01\ Z$, i.e., directly from the observed surface temperature. By contrast, the height and maximum temperature T_M of the inversion are known at best imperfectly, even as averages.

Their most detailed study was carried out by Phillpot & Zillman (1970) who showed the monthly mean inversion strength $I = T_M - T_0$ at Antarctic stations to be related, throughout the year, to their monthly mean surface temperatures. This made it possible to represent the inversion strength in terms of deviations from the means for January, the month in which the inversion is weakest everywhere. Thus

$$I = T_M - T_0 = I_{Jan} + \Delta T_0 - \Delta T_M \qquad (7)$$

where ΔT_0 denotes deviations from the January mean surface temperature T_{0Jan}, and ΔT_M deviations from the January (maximum) temperature T_{MJan} above the inversion. Phillpot and Zillman provided the following values for ΔT_M:

Month	1	2	3	4	5	6	7	8	9	10	11	12
ΔT_m °C	0	3.5	7.5	10.5	12	12.5	12	12.5	12	9	5	1.5

Moreover, their data for three stations on the ice sheet

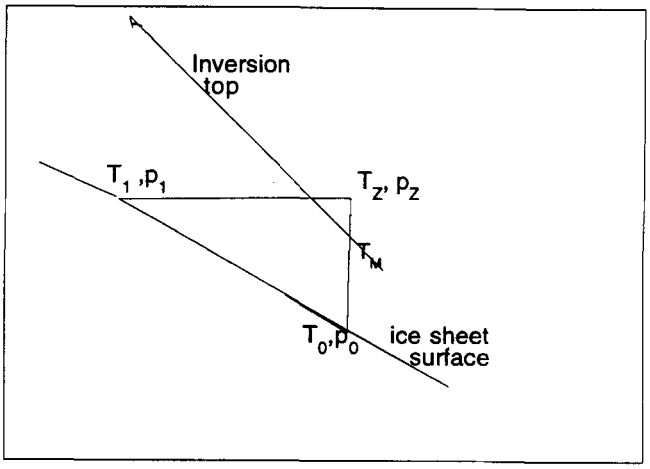

Fig 5. Notation used in the analysis of hydrostatic changes along the ice sheet surface.

suggested that the January inversion strength I_{Jan} is of the order of 2°C everywhere. Thus $T_{MJan} = T_{0Jan} + 2$, and finally

$$T_M = T_{0_{Jan}} - \Delta T_M + 2. \qquad (8)$$

These climatic values of T_M are listed in Appendix B, together with the AWS surface temperatures and pressures and T_{zmin} for 1987, and with the resulting non-hydrostatic residuals there defined.

Above the two coastal stations with regular radiosoundings, observed temperatures T_{zobs} are available for a comparison of T_z estimates. Table III gives three observed monthly temperature means at 240m (the elevation of AWS D10) above Dumont d'Urville, and at 1366 m (the elevation of AWS Law) above Casey; all lie between the T_M of equation (8) and the T_{zmin} for those levels.

Since free-air temperatures are not observed above the AWS themselves, the temperature limits in Tables BI and BII have been used to calculate non-hydrostatic residuals of the changes in surface pressure between adjacent AWS. Pairs of residuals Δp_{min} and Δp_{max}, calculated with T_M and T_{zmin}, respectively, are given in Appendix B. The T_{zmin} lead to physical upper limits for the Δp_{max}, whereas smaller Δp_{min} than those computed with the climatically based T_M can arise when, as in this case, a single year is considered.

Table III. Observed and estimated free-air temperatures.

Month 1987		January	June	October
Dumont d'Urville	T_M	275.3	262.8	266.3
	T_{Zobs}	271.8	260.5	261.6
	T_{Zmin}	271.3	258.7	260.5
Casey	T_M	276.7	264.2	267.7
	T_{Zobs}	266.3	258.0	258.1
	T_{Zmin}	261.1	249.3	251.1

https://doi.org/10.1017/S0954102096000284 Published online by Cambridge University Press

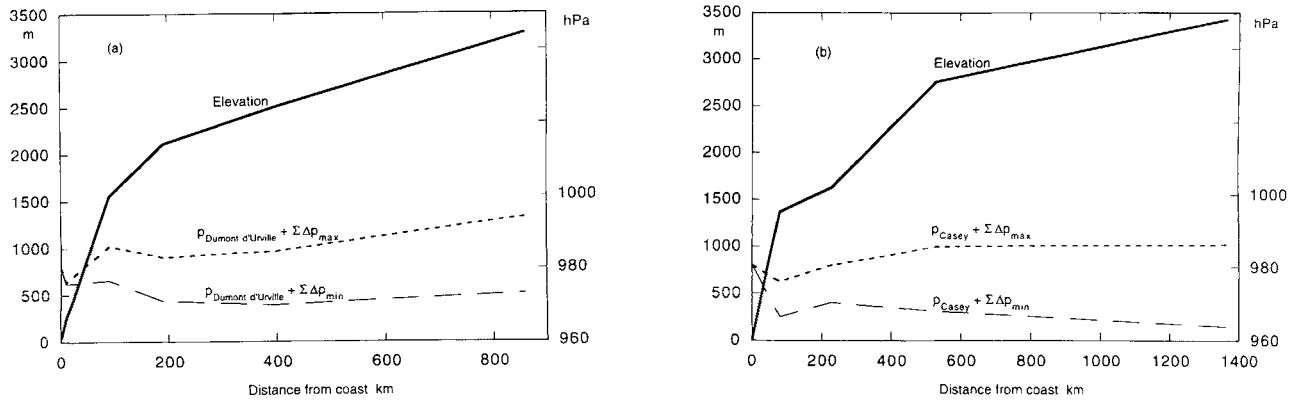

Fig. 6. Elevation-free ("sea level") pressures obtained by adding progressive sums of the annual mean non-hydrostatic residuals Δp of Appendix B to the annual mean surface pressures at **a.** Dumont d'Urville. **b.** Casey.

Discussion

Pressure residuals as large as those in Appendix B could arise simply from instrumental differences, especially where AWS pressures are compared with pressures recorded at manned stations. This is contradicted by systematic changes which are found along both AWS lines. Another instrumental effect, a possible lowering of the recorded pressure in strong winds, could be suspected for the negative pressure residuals at both near-coastal AWS sites; but the wind speeds recorded on Law Dome and at D10 are not significantly higher than at other AWS sites.

As final step the annual averages of the non-hydrostatic pressure residuals Δp in Appendix B have been added consecutively to the mean pressures at Dumont d'Urville and Casey to define pairs of average altitude-corrected ("sea level") pressure profiles over the ice sheet (Fig. 6). At least in principle these pressures, derived with a procedure analogous to the "differential" construction of constant pressure surfaces, would not be subject to the objections which can been raised (e.g. Schwerdtfeger 1984) against the traditional reduction of elevated pressures to sea level. But the uncertain inversion characteristics lead to a wide spread between the pairs of profiles.

Near the coast the altitude-corrected pressures on the ice sheet, even those which represent upper limits due to the use of T_{zmin} in the computation of Δp, show troughs in both AWS lines. Inland Dome C, a high point of the ice sheet, has clear positive anomalies in both profiles throughout the year; at Vostok, 300 km downslope from the crest, a negative annual mean pressure residual results for T_M only.

Positive residuals on the central ice sheet point to a "glacial anticyclone", such as that inferred by Alfred Wegener from observations during the 1912 crossing of the Greenland ice sheet (Koch & Wegener 1930). This received wide discussion (e.g. Hobbs 1945) but became discredited, at any rate for Greenland. Its existence in Antarctica, together with that of a coastal trough, could be understood as resulting from the tropospheric circulation maintaining the strong katabatic drainage of surface air from the ice sheet. This possibility will need to be studied further, with non-hydrostatic residuals based on more extensive data for this and other regions of Antarctica, and with improved information on the inversion strength and thickness which play crucial roles in the dependence of surface pressure on ice sheet elevation.

Acknowledgements

Support for this work has been provided by NSF Grant DPP 90-17969 for "Project Bora", and by the Australian Antarctic Division. We are also indebted to Bob Dattore of NCAR for the results of radiosoundings made from Casey during 1987, and to Barbara Sloan for producing the manuscript. Comments and suggestions from William Connolley and Thomas Parish have helped substantially to improve an earlier version of the paper.

References

Allison, I. & Morrissy, J.V. 1983. Automatic weather stations in the Antarctic. *Australian Meteorological Magazine*, **31**, 71–76.

Allison, I., Wendler, G. & Radok, U. 1993. Climatology of the East Antarctic ice sheet (100 E to 140 E) derived from automatic weather stations. *Journal of Geophysical Research*, **98** (D5), 8815–8823.

Dalrymple, P.C., Lettau, H.H. & Wollaston, S. 1966. South Pole Meteorology Program: Data analysis. *Antarctic Research Series*, **9**, 13–58.

Hobbs, W.H. 1945. The Greenland glacial anticyclone. *Journal of Meteorology*, **1**, 143–153.

Jenssen, D. & Radok, U. 1982. On the joint interpretation of total gas contents and stable isotope ratios in ice cores. *Annals of Glaciology*, **3**, 152–155.

Koch, J.P. & Wegener, A. 1930. Wissenschaftliche Ergebnisse der Dänischen Expedition nach Dronning Louises-Land und quer über das Inlandeis von Nord-Groenland 1912–13, unter Leitung von Hauptmann. *Meddelelser om Grønland*, **75**, 1-676.

Meehl, G.A. 1991. A re-examination of the mechanism of the semi-annual oscillation in the Southern Hemisphere. *Journal of Climate*, **4**, 911-926.

Meinardus, W. 1909. Die mutmassliche Hoehe des antarktischen Kontinents.

Petermanns geographische Mitteilungen, **55**, 304-309 & 355–360.

PHILLPOT, H.R. & ZILLMAN, J.W. 1970. The surface inversion over the Antarctic continent. *Journal of Geophysical Research*, **75** , 4161–4169.

RADOK, U. 1981. The lower atmosphere of the polar regions. *Geologische Rundschau*, **70**, 703–724.

RADOK, U., BROWN, T.J., JENSSEN, D., SMITH, I.N. & BUDD, W.F. 1986. On the surging potential of polar ice streams, part IV: Antarctic ice accumulation basins and their main discharge regions. *Report DE/ER/60197-5 for U.S. Department of Energy*. Cooperative Institute for Research in Environmental Sciences (CIRES), University of Colorado/Boulder and Meteorology Department, University of Melbourne.

SCHWERDTFEGER, W. 1984. *Weather and climate of the Antarctic*. New York: Elsevier Science, 261 pp.

SCHWERDTFEGER, W. & PROHASKA, F. 1956. The semi-annual pressure oscillation, its cause and effects. *Journal of Meteorology*, **13**, 217–218.

TZENG, R.-Y., BROMWICH, D.H. & PARISH, T.R. 1993. Present-day Antarctic climatology of the NCAR Community Climate Model Version 1. *Journal of Climate*, **6**, 205–226.

VAN LOON, H. 1967. The half-yearly oscillation in middle and high southern latitudes, and the coreless winter. *Journal of the Atmospheric Sciences*, **24**, 472–486.

WENDLER, G., KODAMA, Y. & GOSINK, J.P. 1986. Automatic weather stations in East Antarctica. *Antarctic Journal of the United States*, **19** (5), 212–213.

WENDLER, G. & POOK, M. 1992. On the half-yearly pressure oscillation in eastern Antarctica. *Antarctic Journal of the United States 1992*, **27** (5), 284–285.

Appendix A

Atmospheric pressure along a sloping surface.

The change in surface pressure along a slope must balance the effects of two temperature lapse rates—the vertical gradient $\gamma = \delta T/\delta z$ and the "topographical" gradient $\Gamma = \delta T/\delta E$, where z is the vertical coordinate and E is the surface elevation. To clarify this balance it is convenient to start from a level Z above the surface where the pressure and (absolute) temperature have the values p_z and T_z. The hydrostatic equation $dp = g\rho dz$ for that level takes the form

$$\frac{\partial p_Z}{\partial Z} = -gp_z / RT_z \qquad \text{(A1)}$$

where g is the acceleration of gravity, R the specific gas constant of air, and $-g/R = -0.0341$°C/m is the lapse rate of a constant-density atmosphere. Integration from the surface ($z = 0$) to Z and solving for p_0 gives

$$p_0 = p_z\left[1+\frac{\gamma Z}{T_0}\right]^{\frac{g}{R\gamma}}. \qquad \text{(A2)}$$

Then the pressure change along the surface is

$$\frac{\partial p_0}{\partial E} = \frac{\partial p_z}{\partial E}\left[1+\frac{\gamma Z}{T_0}\right]^{\frac{g}{R\gamma}} + p_z\left[\frac{g}{R\gamma}\right]\left[1+\frac{\gamma Z}{T_0}\right]^{\frac{g}{R\gamma}}\left[1+\frac{\gamma Z}{T_0}\right]^{-1}\left[-\frac{\gamma Z}{T_0^2}\frac{\partial T_0}{\partial E}\right]. \qquad \text{(A3)}$$

From Fig. 5.

$$Z\frac{\partial T_0}{\partial E} = \Gamma Z = T_1 - T_0 \text{ and also } p_Z\left[1+\frac{\Gamma Z}{T_0}\right]^{\frac{g}{R\gamma}} = p_0.$$

Moreover, $\delta p_z/\delta E = gp_z/RT_z$ so that (A3) becomes

$$\frac{\partial p_0}{\partial E} = -\frac{gp_0}{RT_z} + \frac{gp_0}{R}\left[\frac{T_0 - T_1}{T_0^2 + \gamma Z T_0}\right] = -\frac{gp_0}{R}\left[\frac{1}{T_z} - \frac{(1 - T_1/T_0)}{T_0 + \gamma Z}\right]$$

and since $T_0 + \gamma Z = T_z$ we get finally an *isothermal* hydrostatic equation,

$$\frac{\partial p_0}{\partial E} = -\frac{gp_0}{RT_0}\frac{T_1}{T_Z} = -\frac{gp_0}{RT^*} \qquad \text{(A4)}$$

where

$$T^* = T_0\frac{T_Z}{T_1}.$$

Jenssen and Radok obtained (A4) as an approximation, but the above derivation shows it to be exact. With a vertical surface inversion and a surface temperature decrease with elevation (the usual ice sheet conditions) $T_z > T_0 > T_1$, so that $T_1/T_z < 1$ and the pressure decrease along the surface is slower than the simple hydrostatic rate $\delta p_0/\delta E = -gp_0/RT_0$, creating a down-slope flow. On the other hand, with vertical lapse ($\gamma < 0$) and slope heating so that $\Gamma > 0$ we have $T_0/T_z > 1$, and the surface pressure decreases with elevation at a faster rate than the simple hydrostatic one. This gives rise to the daytime up-slope valley wind.

Appendix B

The following tables present the data used to calculate non-hydrostatic pressure residuals between adjacent AWS. Each AWS/month box contains the following information:

p_0	T_0
Δp_{max}	T_{zmin}
Δp_{min}	T_M

where p_0 = surface pressure (hPa), T_0 = surface temperature (°K-200), T_M = (estimated) temperature at the upper inversion boundary, and $T_{zmin} = T_0 - 0.01\Delta E$. With subscript 1 for the corresponding information in the next box for the same month, its non-hydrostatic residuals are given by

$$p_1 - p_h = \Delta p = p_1 - p_0 \exp(-0.341\Delta E / T^*)$$

with $T^* = T_0 T_M / T_1$ for Δp_{min},

and $T^*_{min} = T_0 T z_{min} / T_1$ for Δp_{max}

https://doi.org/10.1017/S0954102096000284 Published online by Cambridge University Press

Table BI. Data used to calculate non-hydrostatic pressure residuals: IAGO Line (see text for key).

Month	Dumont d'U		D10		D47		D57		D80		DMC	
1987	pressure	temp	pressure	temp	pressure	temp	pressure	temp	pressure	temp	pressure	temp
Jan	982.7	73.3	960.9	71.2	821.7	61.1	763.6	56.8	725.6	51.3	658.9	45.2
	-	71.3	2.0	69.2	3.8	55.6	-1.3	52.8	0.8	43.5	6.7	-
	-	75.3	1.8	73.2	1.9	63.1	-2.9	58.8	0.0	53.3	4.0	-
Feb	982.7	69.9	951.9	67.0	813.7	57.3	754.3	51.7	716.0	41.2	647.8	32.7
	-	67.9	-6.7	53.8	11.4	51.8	-2.7	47.7	0.0	33.4	6.4	-
	-	71.8	-7.0	69.7	3.3	59.6	-4.3	55.3	-1.1	49.8	1.8	-
Mar	978.6	64.1	949.0	61.1	808.7	49.5	748.9	44.3	711.2	32.7	644.0	22.1
	-	62.1	-5.1	47.9	10.9	44.0	-1.6	40.3	1.3	24.9	8.8	-
	-	67.8	-5.6	65.7	1.5	55.6	-4.2	51.3	-0.4	45.0	2.6	-
Apr	984.0	59.9	953.9	57.0	810.8	45.2	750.0	37.5	711.6	22.8	643.4	12.4
	-	57.9	-5.0	43.8	11.3	40.2	-2.1	33.5	1.2	15.0	11.0	-
	-	64.8	-5.7	62.7	0.8	52.6	-5.0	48.3	-1.1	42.8	2.4	-
May	975.4	56.5	948.0	53.8	803.8	41.2	743.4	33.7	706.9	20.9	641.1	8.4
	-	54.6	-2.2	40.6	10.3	35.8	-1.2	29.7	3.7	13.1	12.8	-
	-	63.3	-3.0	61.2	-0.9	51.1	-4.7	46.8	0.9	41.3	4.1	-
Jun.	989.4	60.7	959.4	59.4	815.6	48.2	750.9	41.4	717.7	31.8	650.7	19.0
	-	58.7	-4.7	46.2	10.2	42.7	-6.1	37.4	6.7	24.0	12.8	-
	-	62.8	-5.1	60.7	2.4	50.6	-7.9	46.3	5.3	40.8	4.2	-
Jul.	984.4	55.9	957.3	54.4	811.8	43.2	750.0	34.1	713.1	23.1	646.9	10.2
	-	53.9	-1.5	41.2	11.0	37.7	-2.9	30.1	3.9	15.3	12.2	-
	-	63.3	-2.4	61.2	0.0	51.1	-5.9	46.8	1.2	46.3	2.8	-
Aug	969.4	54.7	939.1	52.1	794.5	40.6	732.1	31.4	695.3	17.3	627.4	3.5
	-	52.7	-5.1	38.9	10.0	35.1	-3.9	27.4	2.9	9.5	10.1	-
	-	62.8	-6.0	60.7	-1.9	50.6	-7.5	46.3	-0.1	40.8	0.5	-
Sep	974.5	58.6	948.8	56.1	805.5	45.1	739.9	41.8	708.6	28.5	644.2	16.4
	-	56.6	-0.7	43.2	10.9	39.6	-6.2	39.6	7.3	20.7	12.1	-
	-	63.3	-1.3	61.2	1.0	51.1	-8.8	46.0	6.3	41.3	0.5	-
Oct	978.5	62.5	946.7	60.9	806.4	50.0	(ΔE = 940 m)		708.0	36.3	640.0	27.1
	-	60.5	-7.0	47.7	11.1	40.6			-2.9	28.5	7.0	-
	-	66.3	-7.5	64.2	2.4	54.1			-7.7	44.3	2.3	-
Nov	978.6	65.8	950.5	64.9	808.0	52.6			709.7	37.9	643.0	31.9
	-	63.8	-3.5	51.7	6.6	43.2			-3.9	30.1	9.0	-
	-	70.3	-4.1	60.2	-1.9	58.1			-9.0	48.3	3.7	-
Dec	985.7	70.9	954.7	68.7	816.2	58.4			718.3	47.3	651.7	43.6
	-	68.9	-6.8	55.5	10.4	49.0			-3.2	37.5	7.9	-
	-	73.8	-7.2	71.7	2.2	61.6			-7.5	51.8	4.4	-
					Annual averages ± standard deviations							
	988.3	Δp_{max}	-3.9 ± 0.8		9.8 ± 0.7		-3.1 ± 0.6		1.5 ± 1.1		9.8 ± 0.7	
		Δp_{min}	-4.4 ± 0.8		0.9 ± 0.5		-5.7 ± 0.6		-1.1 ± 1.4		2.8 ± 0.4	

Elevation difference (ΔE) Durmont d'Urville – D10 = 197 m
D10 – D47 = 1320 m
D47 – D57 = 545 m
D57 – D80 = 395 m
D80 – DMC = 780 m

https://doi.org/10.1017/S0954102096000284 Published online by Cambridge University Press

Table BII. Data used to calculate non-hydrostatic pressure residuals: ANARELine (see text for key).

Month	Casey		Law		A028		GC41		Vostok	
1987	pressure	temp	pressure	temp	pressure	temp	pressure	temp	pressure	temp
Jan	991.2	74.7	831.5	63.2	808.6	59.9	701.0	49.5	639.0	42.2
	-	61.1	-5.1	60.6	4.5	48.6	4.6	42.9	-1.6	-
	-	76.7	-13.1	65.2	4.1	61.9	-0.7	51.5	-3.5	-
Feb	984.1	71.6	873.8	60.1	800.0	53.4	690.9	37.0	628.0	27.7
	-	58.0	-5.1	57.5	3.3	42.1	2.3	31.2	-1.4	-
	-	73.2	-13.1	61.7	2.9	50.4	-4.2	40.0	-5.3	-
Mar	980.1	66.3	816.7	54.0	793.3	46.5	685.9	28.8	624.0	16.1
	-	52.7	-6.5	51.4	4.0	35.2	5.0	22.2	0.8	-
	-	69.2	-15.3	57.7	3.4	54.4	-2.9	44.0	-4.5	-
Apr	983.1	62.5	878.1	51.3	794.8	42.2	686.9	23.1	623.0	9.0
	-	48.9	-4.9	48.7	4.3	30.9	5.8	16.5	-0.1	-
	-	66.2	-14.4	54.7	3.6	51.4	-2.8	41.0	-6.2	-
May	981.1	58.3	817.7	46.7	794.2	37.4	682.8	20.1	623.0	6.5
	-	44.7	-1.4	44.1	4.5	26.1	5.1	13.5	4.6	-
	-	64.7	-12.6	53.2	3.5	49.9	-5.2	39.5	-2.0	-
Jun	980.1	62.9	817.3	51.4	795.9	47.9	690.3	31.7	630.0	13.5
	-	49.3	-3.6	48.8	6.7	36.6	7.1	25.1	0.5	-
	-	64.2	-11.8	52.7	6.3	49.4	1.8	39.0	-2.8	-
Jul	985.1	61.6	820.4	48.9	796.7	40.9	689.0	20.8	628.0	7.4
	-	48.0	-4.7	46.3	4.3	29.6	6.4	14.2	3.8	-
	-	64.7	-14.0	53.2	3.5	49.9	-2.3	39.5	-2.6	-
Aug	971.0	51.5	802.0	40.5	778.7	32.8	670.1	12.9	607.0	-2.1
	-	37.9	-4.4	37.9	5.1	21.5	6.3	6.3	1.6	-
	-	64.2	-19.4	52.7	3.4	49.4	-5.6	39.0	-6.8	-
Sep	976.1	60.3	814.7	49.2	792.1	43.5	682.0	28.7	624.0	6.2
	-	46.7	-1.1	46.6	5.4	32.2	4.6	22.1	1.6	-
	-	64.7	-11.1	53.2	4.8	49.9	-2.9	39.5	-2.5	-
Oct	974.1	64.7	811.3	54.1	787.9	48.9	680.4	32.1	619.0	16.9
	-	51.1	-5.0	51.5	4.1	37.6	3.5	25.5	-0.7	-
	-	67.7	-14.0	56.2	3.6	52.9	-2.7	42.5	-4.7	-
Nov	976.1	60.7	815.0	55.7	792.2	51.2	685.5	36.7	623.0	28.0
	-	55.1	-6.5	53.1	4.7	39.9	5.0	30.1	-0.8	-
	-	71.7	-15.2	60.2	4.0	56.9	-1.9	46.5	-4.7	-
Dec	985.7	73.3	824.5	61.4	801.4	58.0	694.1	47.2	632.0	40.7
	-	59.7	-7.0	58.8	4.3	46.7	4.5	40.6	-1.6	-
	-	75.2	-15.0	63.7	3.8	60.4	-0.9	50.0	-3.7	-
					Annual averages ± standard deviations					
	980.6	Δp_{max}	-4.6 ± 0.5		4.6 ± 0.3		5.0 ± 0.4		0.6 ± 0.6	
		Δp_{min}	-14.1 ± 0.6		4.6 ± 0.3		-2.5 ± 0.6		-4.1 ± 0.4	

Elevation difference (ΔE) Casey – Law = 1355 m
Law – A028 = 259 m
A028 – GC41 = 1134 m
GC41 – Vostock = 661 m

https://doi.org/10.1017/S0954102096000284 Published online by Cambridge University Press